

Computational dynamics of acoustically driven microsphere systems

Connor Glosser,^{1,2,*} Carlo Piermarocchi,^{1,†} Jie Li,² Dan Dault,² and B. Shanker²

¹*Department of Physics & Astronomy, Michigan State University, Biomedical Physical Sciences,
567 Wilson Road, East Lansing, Michigan 48824, USA*

²*Department of Electrical & Computer Engineering, Michigan State University, Engineering Building,
428 S. Shaw Lane, East Lansing, Michigan 48824, USA*

(Received 31 August 2015; revised manuscript received 10 December 2015; published 15 January 2016)

We propose a computational framework for the self-consistent dynamics of a microsphere system driven by a pulsed acoustic field in an ideal fluid. Our framework combines a molecular dynamics integrator describing the dynamics of the microsphere system with a time-dependent integral equation solver for the acoustic field that makes use of fields represented as surface expansions in spherical harmonic basis functions. The presented approach allows us to describe the interparticle interaction induced by the field as well as the dynamics of trapping in counter-propagating acoustic pulses. The integral equation formulation leads to equations of motion for the microspheres describing the effect of nondissipative drag forces. We show (1) that the field-induced interactions between the microspheres give rise to effective dipolar interactions, with effective dipoles defined by their velocities and (2) that the dominant effect of an ultrasound pulse through a cloud of microspheres gives rise mainly to a translation of the system, though we also observe both expansion and contraction of the cloud determined by the initial system geometry.

DOI: [10.1103/PhysRevE.93.013305](https://doi.org/10.1103/PhysRevE.93.013305)

I. INTRODUCTION

Computational approaches that employ an integral equation formalism to examine acoustic scattering from particles typically assume a static environment in which scatterers remain stationary. At present, a large body of work details such scattering problems [1–3]. While these stationary integral equation methods offer a large degree of accuracy in capturing the underlying physics, many problems of interest require a fully dynamical treatment. For instance, in biomedical physics, gas-filled microspheres exposed to ultrasonic beams have demonstrated effectiveness as a contrast imaging agent [4] and as drug delivery method [5,6], and Ding *et al.* have demonstrated their manipulation using acoustic tweezers in microfluidic channels [7]. Moreover, composite materials consisting of colloidal in-fluid suspensions have peculiar sound propagation properties that can deviate from the ones of homogeneous liquids [8]. In each of these applications, the unconstrained motion of scatterers requires a self-consistent description of their dynamics in conjunction with a description of the acoustic field propagation.

Here we demonstrate the applicability of coupling particle kinetics to a time-domain integral equation scattering framework to model rigid-sphere motion induced by a time-dependent acoustic potential. Specifically, we consider the case of an acoustic pulse acting on microspheres that move in a fluid. Effective Langevin time-averaged radiation pressure forces [9,10], which consider the case of a steady radiation flux incident on a body kept in static equilibrium, do not provide an appropriate model in this case as they cannot accommodate interparticle scattering effects. While many

theoretical and computational descriptions of higher-order acoustic interactions exist [11–15], few actually make use of computed fields to predict particle trajectories. As we consider only short-duration pulses, we refrain from time averaging in favor of using a time-domain scattering formulation to explicitly calculate particle trajectories resulting from a prescribed pulse. By adopting a weakly compressible potential formulation of the fluid media, our scalar wave problem inherits a number of similarities and solution techniques from scattering problems in electromagnetic theory, a topic previous works discuss extensively [11,16,17]. Moreover, our time-domain formulation readily allows the study of transient phenomena (such as acoustic tweezing), a convenience not shared with more common frequency domain approaches.

We structure the remainder of this paper as follows: We first provide a formal mathematical description of the problem—including details on both the kinetic and field methods—followed by data obtained from various pulse and microsphere configurations, demonstrating both attractive and repulsive regimes suitable for subtle control of spherical systems in a homogeneous fluid. Finally, we offer concluding remarks on the effectiveness of the simulation as well as our thoughts on possible future extensions.

II. CONTINUUM PROBLEM STATEMENT

Consider a collection of N rigid, nonintersecting spherical scatterers (microspheres), each having radius a_k , position \mathbf{x}_k , and enclosing volume $V_k \subset \mathbb{R}^3$ (Fig. 1). The microspheres move in a homogeneous exterior fluid occupying V_E , where we denote the boundary of each microsphere as $\Omega_k = \partial V_k$ and thus may ascribe to each an outward-pointing normal $\hat{\mathbf{n}}_k(\theta, \phi)$, where θ and ϕ represent colatitude and azimuthal angles with respect to the local origin (microsphere center).

*glosser1@msu.edu; <http://www.msu.edu/~glosser1>.

†carlo@pa.msu.edu

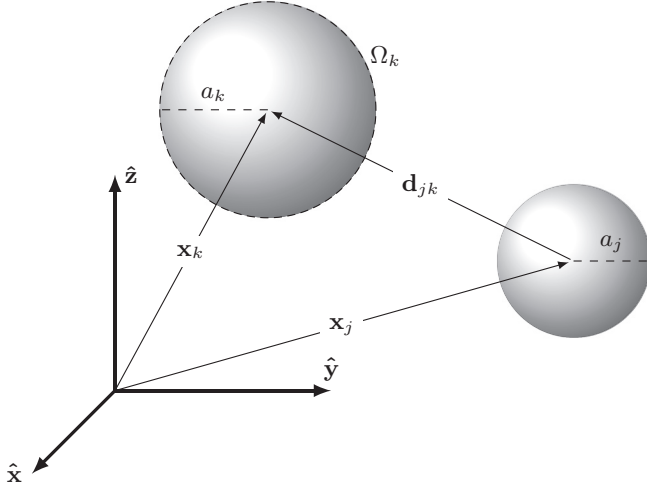


FIG. 1. Coordinate notation.

We wish to investigate the reaction of the system to an incident acoustic pulse, thus the fluid carries a prescribed (band-limited) waveform through the microsphere system in which it interacts with each of the $\partial\Omega_k$ according to the “sound-hard” regime presented in [17]. The incident acoustic pulse, in combination with the acoustic field scattered from each microsphere and the hydrodynamic field induced by the

relative velocity of each microsphere, acts as a perturbation to the initially at-rest uniform ideal fluid [18,19]. We consider here the linear regime, in which the perturbation induced by the acoustic and aerodynamic contribution remain sufficiently small so the velocity field $\mathbf{v}(\mathbf{x},t)$ satisfies the condition $|\mathbf{v}(\mathbf{x},t)| \ll c_s$, where c_s represents the speed of sound in the fluid. In this limit, the velocity potential, defined by $\mathbf{v}(\mathbf{x},t) = \nabla\varphi(\mathbf{x},t)$, satisfies the scalar wave equation:

$$\left(\frac{1}{c_s^2} \frac{\partial^2}{\partial t^2} - \nabla^2\right)\varphi(\mathbf{x},t) = 0, \quad (1)$$

and we may express the pressure perturbation at any point in the exterior medium as

$$p(\mathbf{x},t) = -\rho_0 \frac{\partial\varphi(\mathbf{x},t)}{\partial t}, \quad (2)$$

where ρ_0 denotes the equilibrium density of the fluid. Rigidity of the Ω_k necessarily prescribes boundary conditions on the normal velocity components at each interface, namely

$$\left.\frac{\partial\varphi(\mathbf{x},t)}{\partial \hat{\mathbf{n}}_k}\right|_{\mathbf{x} \in \Omega_k} = \frac{d\mathbf{x}_k}{dt} \cdot \hat{\mathbf{n}}_k, \quad (3)$$

where \mathbf{x}_k represents the center-of-mass coordinate for the k^{th} microsphere.

Using these relations, we apply the Kirchoff-Helmholtz theorem to define the following system of integral equations:

$$\varphi(\mathbf{x},t) = \varphi_{\text{inc}}(\mathbf{x},t) + \sum_{i=0}^{N-1} \int dt' \int_{\Omega_k(t')} dA \left[\varphi(\mathbf{x}',t') \frac{\partial G_r(\mathbf{x},t; \mathbf{x}',t')}{\partial \hat{\mathbf{n}}_k} - G_r(\mathbf{x},t; \mathbf{x}',t') \frac{\partial \varphi(\mathbf{x}',t')}{\partial \hat{\mathbf{n}}_k} \right], \quad (4)$$

where $G_r(\mathbf{x},t; \mathbf{x}',t')$ denotes the Green’s function for a retarded potential,

$$G_r(\mathbf{x},t; \mathbf{x}',t') = \frac{\delta(t - t' - |\mathbf{x} - \mathbf{x}'|/c_s)}{4\pi |\mathbf{x} - \mathbf{x}'|}. \quad (5)$$

If the system remains localized to a region with small dimensions when compared to the wavelength of sound, then retardation effects become negligible and we may instead use the Laplace-kernel Green’s function,

$$G(\mathbf{x},\mathbf{x}') = \frac{1}{4\pi |\mathbf{x} - \mathbf{x}'|}. \quad (6)$$

To ease notation, we define the following two integral operators:

$$\hat{\mathcal{S}}_k[\varphi(\mathbf{x} \in \Omega_k(t),t)] = \int_{\Omega_k(t)} dA G(\mathbf{x},\mathbf{x}') \partial_{\hat{\mathbf{n}}_k} \varphi(\mathbf{x}',t), \quad (7a)$$

$$\hat{\mathcal{D}}_k[\varphi(\mathbf{x} \in \Omega_k(t),t)] = \int_{\Omega_k(t)} dA \varphi(\mathbf{x}',t) \partial_{\hat{\mathbf{n}}_k} G(\mathbf{x},\mathbf{x}'), \quad (7b)$$

reducing Eq. (4) to

$$\varphi(\mathbf{x},t) = \varphi_{\text{inc}} + \sum_{k=0}^{N-1} (\hat{\mathcal{D}}_k - \hat{\mathcal{S}}_k)[\varphi(\mathbf{x} \in \Omega_k(t),t)]. \quad (8)$$

In solving Eq. (8), we obtain the velocity potential everywhere for a given time without retarded scattered fields. For the incident pulse, φ_{inc} , we consider superpositions of wave packets of the form

$$\varphi_{\text{inc}}(\mathbf{x},t) = P_0 \cos(\omega_0 t - \mathbf{k} \cdot \mathbf{x}) e^{-(c_s t - \hat{\mathbf{k}} \cdot \mathbf{x})^2 / (2\sigma^2)}. \quad (9)$$

Finally, the variation in pressure (and thus φ) over each of the Ω_k necessarily propels each microsphere according to the equation of motion,

$$m_k \frac{d^2 \mathbf{x}_k}{dt^2} = \rho_0 \int_{\Omega_k(t)} dS \frac{\partial \varphi(\mathbf{x},t)}{\partial t}. \quad (10)$$

III. DISCRETIZATION OF THE INTEGRAL EQUATIONS

To solve the integral equation scattering problem, we begin by discretizing our field in both space and time. As we have restricted our particles to completely spherical geometries, the spherical harmonics, defined by

$$Y_{\ell m}(\theta, \phi) = \sqrt{\frac{2\ell + 1}{4\pi} \frac{(\ell - m)!}{(\ell + m)!}} P_{\ell}^m(\cos \theta) e^{im\phi}, \quad (11)$$

give simple eigenfunctions of the operators in Eq. (7). As a result, they lend themselves well to an expansion of φ on the surface of each microsphere with respect to the microsphere’s

center,

$$\varphi(\mathbf{x} \in \Omega_k, t) = \sum_{\ell \geq 0} \sum_{|m| \leq \ell} C_{\ell m}^k(t) Y_{\ell m}(\theta, \phi). \quad (12)$$

By considering Eq. (2) and expressing the local velocity potential at each of the Ω_k as a linear combination of spherical harmonics, we have a complete representation of the body force acting on each microsphere,

$$\begin{aligned} \mathbf{F}_{\text{body}}^k(t) &= - \int_{\Omega_k(t)} d\mathbf{S} p(\mathbf{x} \in \Omega_k, t) \\ &= \rho_0 \sqrt{\frac{2\pi}{3}} r^2 [(\dot{C}_{11}^k(t) - \dot{C}_{1-1}^k(t)) \hat{\mathbf{x}} \\ &\quad + i[\dot{C}_{11}^k(t) + \dot{C}_{1-1}^k(t)] \hat{\mathbf{y}} - \sqrt{2} \dot{C}_{10}^k(t) \hat{\mathbf{z}}], \end{aligned} \quad (13)$$

due to the orthogonality of dipole terms with the rest of the multipoles.

The problem then becomes one of solving a system of linear equations that we may compactly represent as

$$\overline{\mathcal{Z}} \cdot \boldsymbol{\varphi} = \mathcal{F}, \quad (14)$$

with the overbar denoting a matrix quantity. We define the elements of \mathcal{F} as projections of the incident field onto local spherical harmonics,

$$\mathcal{F}_{\ell m}^k = \int_{\Omega_k(t)} dA Y_{\ell m}^*(\theta, \phi) \varphi_{\text{inc}}(\mathbf{x}, t), \quad (15)$$

and detail $\mathcal{Z}_{\ell m, \ell' m'}^{jk}$ for two cases: $j = k$ and $j \neq k$. In the instances where $j = k$, Eq. (7) propagates effects of the interaction through to every point on a surface sharing a coordinate system with the original, thus the harmonics remain orthogonal and

$$\mathcal{Z}_{\ell m, \ell' m'}^{jj} = \frac{\ell + 1}{2\ell + 1} \delta_{\ell \ell'} \delta_{mm'} \quad (16)$$

after exploiting the well-known expansion theorem for Eq. (6),

$$G(\mathbf{x}, \mathbf{x}') = \sum_{\ell, m} \frac{1}{2\ell + 1} \frac{r_{<}^{\ell}}{r_{>}^{\ell+1}} Y_{\ell m}(\theta, \phi) Y_{\ell m}^*(\theta', \phi'), \quad (17)$$

where $r_{<} = \min(|\mathbf{x}|, |\mathbf{x}'|)$ and $r_{>} = \max(|\mathbf{x}|, |\mathbf{x}'|)$. A description of the off-diagonal terms where $j \neq k$ proceeds much the same way, though the surface expansions no longer share a local origin, complicating the projections. Translation operators for the spherical harmonics [20,21] allow analytic expressions for these matrix elements, though we eschew such operators in favor of numerical integration for speed.

Thus, at every time step of the simulation, the algorithm proceeds as follows: (i) project the incident pulse and surface velocities onto local expansions of spherical harmonics, (ii) propagate scattering effects through space by inverting the operators in Eq. (8), (iii) project these scattered fields onto local spherical harmonics to give a total representation of φ on each surface, and (iv) move each microsphere according to Eq. (10) and advance $t \rightarrow t + \Delta t$. For rigid microspheres only $\ell = 1$ terms contribute to center-of-mass motion, thus we use only the C_{1m} coefficients in evolving Eq. (10).

The inversion in step (ii) above requires some care; by simply inverting the entire propagation operator, $\hat{D} - \hat{S}$, to

give a single surface pressure, Eq. (10) reduces to a differential equation of the form

$$\dot{\mathbf{x}}_k = f(t, \mathbf{x}_k, \dot{\mathbf{x}}_k). \quad (18)$$

This presents a number of irregularities with conventional integration schemes and will rapidly diverge towards $\pm\infty$ due to the additional $\dot{\mathbf{x}}_k$ on the right if implemented naively. To remedy this, we note that \hat{S} serves to produce *only* a reaction or drag term on each microsphere that impedes motion. By maintaining quantities for the inversion of \hat{D} and \hat{S} separately, we remove the explicit dependence on $\dot{\mathbf{x}}_k$ by introducing a linear coefficient in the form of an additional mass term—given by the $\dot{\mathbf{x}}_k$ -dependent contribution in the single-layer \hat{S} operator—when solving Eq. (10).

IV. ANALYTIC RESULTS

A. Single microsphere solution

As an example, consider a single sphere of density ρ_s and radius a . Taking $ka \ll 1$, we may approximate Eq. (9) as $\varphi_{\text{inc}}(\mathbf{x}, t) = v_0(t)z$ and we wish to find the response velocity of the sphere, \mathbf{u} , in terms of the field velocity $\mathbf{v} = \nabla \varphi_{\text{inc}}$. It follows that the expansion of φ_{inc} contains only $\ell = 1$ terms, thus

$$\varphi_{\text{inc}} = v_0(t) a \cos(\theta) \quad (19)$$

on the surface of the sphere. Similarly, from Eq. (3),

$$\begin{aligned} \partial_{\hat{\mathbf{n}}} \varphi &= \mathbf{u} \cdot \hat{\mathbf{n}} \\ &= u_z a \cos(\theta) \end{aligned} \quad (20)$$

due to the symmetries present in x and y . As a result,

$$\begin{aligned} \varphi - \int dS' \varphi(\mathbf{x}') \partial_{\hat{\mathbf{n}}} G(\mathbf{x}, \mathbf{x}') \\ = v_0 a \cos(\theta) - \int dS' a u_z \cos(\theta) G(\mathbf{x}, \mathbf{x}'), \end{aligned} \quad (21)$$

and it becomes apparent that only $\ell = 1, m = 0$ terms in Eq. (17) remain after integrating. Consequently, the field becomes

$$\varphi(\mathbf{x}, t) = \left[v_0(t) |\mathbf{x}| + \frac{a^3(v_0(t) - u_z)}{2|\mathbf{x}|^2} \right] \cos(\theta) \quad (22)$$

outside the microsphere and

$$\varphi(\mathbf{x} \in \Omega, t) = \left(\frac{3}{2} v_0(t) - \frac{1}{2} u_z \right) a \cos(\theta) \quad (23)$$

on its surface. From this we conclude the total velocity potential in the fluid arises from a surface-scattering term alongside a term describing the transfer of momentum from the moving microsphere to the fluid.

Using Eq. (10), we may then write the equation of motion for the system as

$$\rho_s V \dot{u}_z = \rho_0 V \left(\frac{3}{2} \dot{v}_0 - \frac{1}{2} \dot{u}_z \right). \quad (24)$$

where $V = 4\pi a^3/3$ gives the volume of the microsphere. The transfer of momentum from the moving microsphere to the fluid becomes a reaction force of the fluid due to the sphere. Landau and Lifshitz [19] initially derived this nondissipative

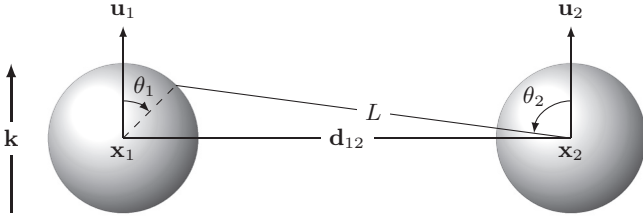


FIG. 2. Perpendicular configuration.

drag force by way of momentum and energy conservation. Note that this drag force presents only in the case of accelerated motion of the microsphere and we may recast its effect in the form of a *virtual mass* that includes a contribution due to the mass of the displaced fluid,

$$\left(\rho_s + \frac{\rho_0}{2}\right)V\dot{u}_z = \frac{3\rho_0 V}{2}\dot{v}_0. \quad (25)$$

This expression leads to a simple relation linking $u_z(t)$ and $v_0(t)$ provided the velocity does not remain constant and that the sphere does not move in the absence of the field:

$$\frac{u_z}{v_0} = \frac{3\rho_0}{\rho_0 + 2\rho_s}. \quad (26)$$

The idea of a virtual mass for the accelerated motion of a single sphere in an ideal fluid readily generalizes to the case of a moving collection of mutually interacting spheres. Through this, we may compute the dynamics of each microsphere in the group, taking into account the effect of the momentum exchange between the fluid and the microspheres, resulting in both drag and interparticle forces in addition to the displacement caused by the driving acoustic field.

B. Low-order interactions

We now consider two identical microspheres arranged perpendicularly to an incident waveform as in Fig. 2. Within the Born approximation, we may take Eq. (19) as the incident field and use it in place of the total field on the right-hand side of Eq. (8), assuming negligible contributions from scattering. In doing so, the field everywhere becomes

$$\begin{aligned} \varphi(\mathbf{x}, t) = & v_0(t)z + \frac{a^3}{3} \frac{\cos(\theta_1)}{|\mathbf{x} - \mathbf{d}_{12}/2|^2} [v_0 - u_1] \\ & + \frac{a^3}{3} \frac{\cos(\theta_2)}{|\mathbf{x} + \mathbf{d}_{12}/2|^2} [v_0 - u_2]. \end{aligned} \quad (27)$$

By inserting this into Eq. (10) for \mathbf{x}_1 , we have

$$\begin{aligned} m_1 \mathbf{u}_1 \cdot \hat{\mathbf{z}} = & 2\pi\rho_0 a^2 \int \cos^2 \theta_1 a^3 \left(\frac{4}{3}v_0 - \frac{u_1}{3}\right) d(\cos \theta_1) \\ & + \rho_0 \int_{\Omega_1} \frac{a^5}{3} \frac{v_0 - u_2}{|\mathbf{x} - \mathbf{d}_{12}|^2} \cos \theta_1 \cos \theta_2 d\phi_1 d(\cos \theta_1). \end{aligned} \quad (28)$$

Writing

$$\cos \theta_2 = \frac{a}{d_{12}} \frac{\cos \theta_1}{\sqrt{\left(1 - \frac{a}{d_{12}} \sin \theta_1\right)^2 + \left(\frac{a}{d_{12}} \cos \theta_1\right)^2}} \quad (29)$$

TABLE I. Typical simulation parameters.

Quantity	Symbol	Value
Sound speed	c_s	1500 ms ⁻¹
Microsphere radius	a_k	1 μm
Density (exterior)	ρ_0	1000 kgm ⁻³
Density (interior)	ρ_s	1 kgm ⁻³
Pulse amplitude	P_0	0.05 m ² s ⁻¹
Center frequency	f_0	0.5 MHz to 20 MHz
Pulse duration (st. dev.)	σ	7 μs to 24 μs

and noting $\mathbf{u}_1 = \mathbf{u}_2 \equiv \mathbf{u}_s$ due to symmetry in the initial configuration, we may expand Eq. (28) in a/d_{12} to give

$$\rho_s u_s = \rho_0 \left(\frac{4}{3}v_0 - \frac{1}{3}u_s\right) + \frac{\rho_0(v_0 - u_s)}{3} \left(\frac{a}{d_{12}}\right)^3. \quad (30)$$

In the limit of $d_{12} \rightarrow \infty$, this becomes

$$\frac{u_s}{v_0} = \frac{4\rho_0}{\rho_0 + 3\rho_s}. \quad (31)$$

By considering negligible scattered fields at the surface of each microsphere, we qualitatively recover Eq. (27) with different coefficients arising only from the Born approximation. Moreover, the additional interaction term in Eq. (31) scales as $|d_{ij}|^{-3}$; a behavior anticipated from the dipolar nature of Eq. (22).

V. NUMERICAL RESULTS

Here we present a series of numerically solved systems to illustrate the utility of the method in investigating acoustic phenomena. We perform simulations of one- and two-particle and/or pulse systems to determine the principal particle-field and particle-particle interactions, followed by simulations of larger assemblages of spheres to investigate group phenomena and effects in systems without symmetry. Unless otherwise stated, Table I gives the simulation parameters for each of the following simulations; as our interests lie in hydrodynamic applications, we use material parameters characteristic of water to define our external fluid medium. Similarly, we consider here the case of gas-filled microspheres [4], and therefore set their density much smaller than that of the exterior medium. The acoustic pulses lie in the ultrasonic regime, and the chosen frequency of 20 MHz corresponds to that of typical applications in acoustic microscopy.

A. Single microspheres

Figure 3 gives the trajectory of a single microsphere initially at rest under the effects of an incident Gaussian pulse. Under the linear and ideal fluid approximations and absent the Gaussian envelope in Eq. (9), the microsphere merely oscillates about its origin in accordance with Eq. (26). In the pulsed case, however, the variation in pressure imposed by the finite value of \mathbf{k} modifies the system dynamics to yield a net translation of each microsphere. Note that the regime considered here produces no net transfer of momentum between the acoustic field and the microsphere—a consequence of the ideal fluid.

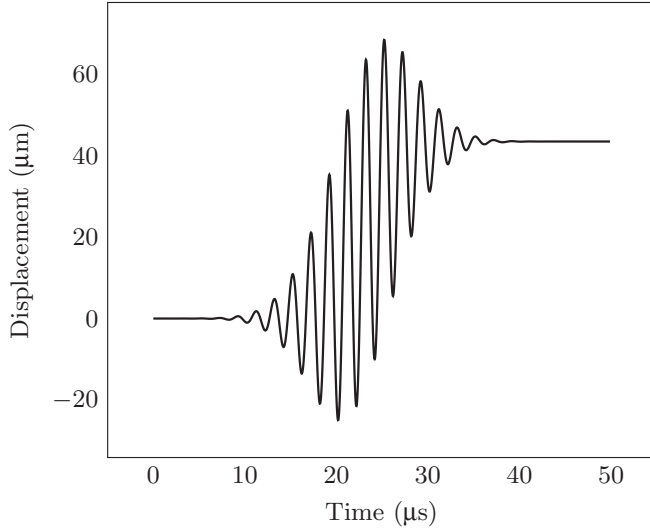


FIG. 3. Translation of a single microsphere interacting with an incident pulse ($f_0 = 0.5$ MHz, $\sigma = 7$ μ s). Microspheres interacting with the pulse translate a finite distance along \mathbf{k} due to the Gaussian envelope in Eq. (9).

Figure 4 depicts smoothed results of 128 trajectories corresponding to single microspheres initially spaced along $\hat{\mathbf{z}}$ and excited by identical counter-propagating pulses. By taking the width of each pulse much greater than the radius of each microsphere, the two pulses reproduce the effects of interfering standing waves. The confinement occurs at $\nabla P = \mathbf{0}$ (nodal) planes where the net force on each microsphere vanishes. The half-wavelength associated with the dominant pulse frequency gives the separation between neighboring planes.

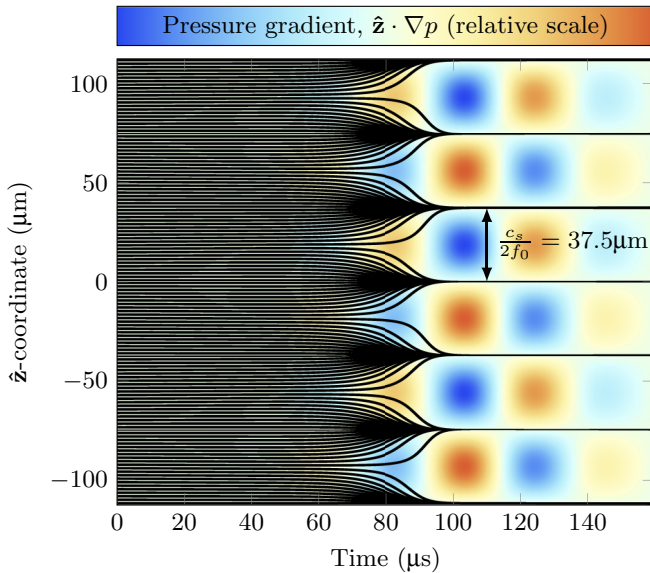


FIG. 4. Confinement of noninteracting spheres to planes; identical counter-propagating pulses ($f_0 = 20$ MHz, $\sigma = 23.8$ μ s) initially displaced along $\hat{\mathbf{z}}$ tend to align objects in $\nabla P = \mathbf{0}$ planes at $\lambda/2$ intervals. Field and trajectories sampled every 30 time steps and smoothed with a 16-sample windowed average.

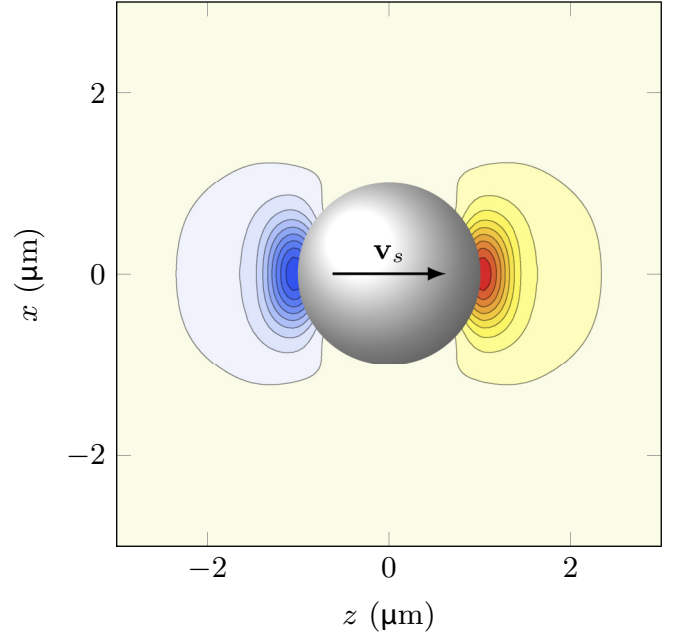


FIG. 5. Calculated isopotential contours near a lone microsphere. Red and blue colorations represent regions of positive and negative potential. The motion of each microsphere through the background medium serves primarily to produce a dipolar field of velocity potential with \mathbf{v}_s serving as the sphere's dipole moment.

Finally, Fig. 5 shows the relative velocity potential near a single microsphere; given a surface expansion of φ , we may compute the potential everywhere through application of Eq. (8). As predicted by Eq. (22), this field greatly resembles that of a pointlike “velocity dipole” with \mathbf{v}_s acting as a dipole moment.

The simulations described thus far demonstrate precise acoustic control; through careful application of the incident field parameters, we may induce a (finite, given a finite pulse) translation along the principal $\hat{\mathbf{k}}$ vector with a large degree of accuracy in the overall displacement. In addition, the application of multiple pulses serves to confine microspheres to highly localized regions in space, offering a self-consistent model of acoustic tweezing.

B. Many-particle simulations

We now turn our attention to collections of mutually interacting microspheres. To quantify the effects of scattering, we first decouple scattering forces from the incident pulse by arranging two microspheres perpendicularly to the pulse's \mathbf{k} vector. Figure 6 gives results for such a simulation where we plot the relative change in velocity as compared with the single-particle simulation,

$$\Delta|\mathbf{v}_{\max}| = \max(|\mathbf{v}_{\text{double}}(t) - \mathbf{v}_{\text{single}}(t)|). \quad (32)$$

In principle, describing quantities found from a complete simulation as a function of initial separation could obfuscate scaling data considerably; forces arising from scattering could alter the geometry of the system. In practice, however, the perpendicular configuration used here gives scattering forces

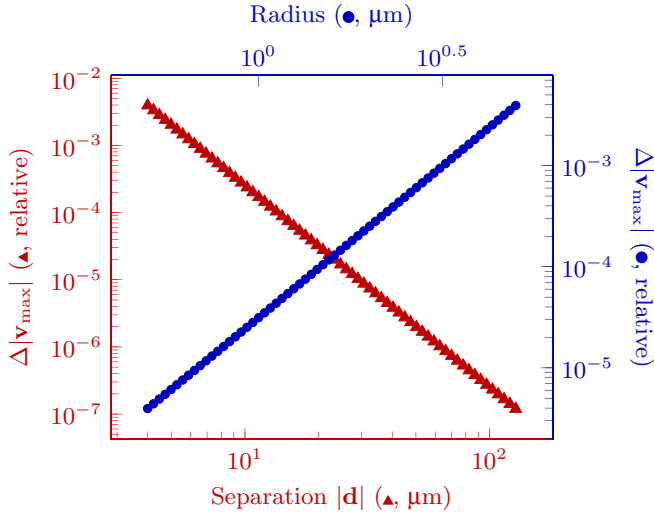


FIG. 6. Scaling behavior of two microspheres arranged perpendicularly to an incident pulse for various radii and initial separations. The \blacktriangle , \bullet symbols on each axis denote data associated with that axis. The \blacktriangle follow a regression of $\Delta|v|_d = 0.250754d_{12}^{-3.00077}$, and the \bullet follow $\Delta|v_{\max}|_r = 3.13328 \times 10^{-5}a_0^{2.99814}$. These trends strongly indicate dominant dipolar interactions between microspheres.

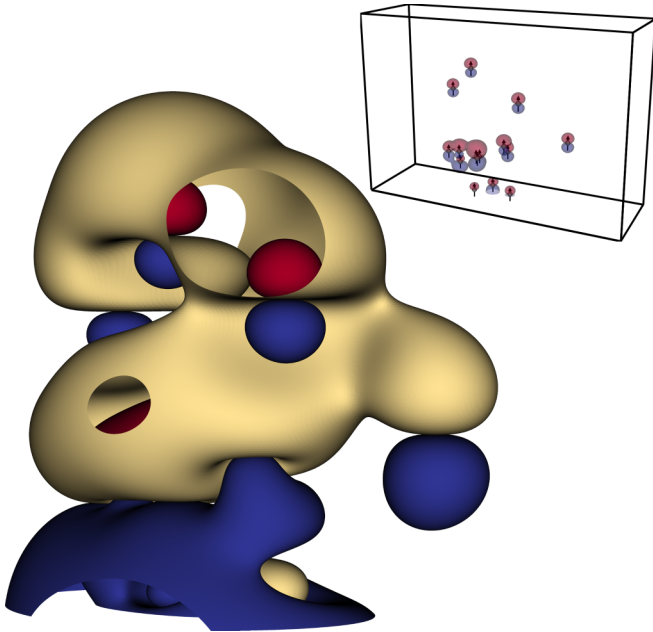


FIG. 7. Isosurfaces of velocity potential (arb. units) calculated by evaluating the \hat{S} and \hat{D} terms in Eq. (8) for a $N = 16$ particle simulation. Red, blue, and yellow surfaces denote regions of positive, negative, and zero potential, with holes appearing due to intersections with the bounding box. The inset box shows the three-dimensional arrangement of the microspheres superimposed with their velocity vectors, as well as several positive and negative potential isosurfaces. Rendered with VisIt [22].

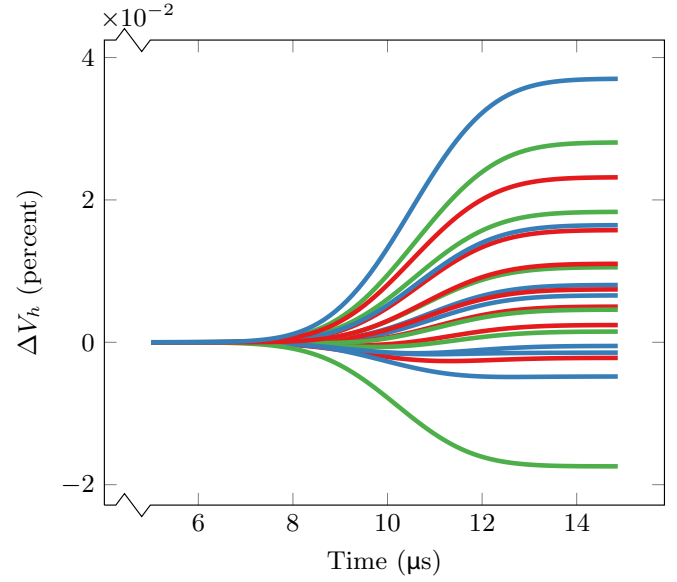


FIG. 8. Fractional change in the volume of 20 randomly initialized microsphere clouds subject to the same incident pulse, smoothed with a 128-sample moving average. Positive and negative values denote expansion and contraction. $\sigma = 1.5$ cm.

that only influence the motion along \mathbf{k} . Consequently, $\Delta\mathbf{v} \propto \mathbf{z}$ and the microspheres' initial separation remains a good estimator of scaling behavior. We see in Fig. 6 that the radii data scale as a_k^3 and the separation data exhibit strong $|d_{12}|^{-3}$ scaling, again indicating a dominant dipolar interaction between microspheres as shown by Ilinskii *et al.* in 2007 [14] and predicted by Eq. (22).

Finally, we consider the dynamics of large ($N = 16$) clouds of microspheres. For each simulation, we generate a collection of microspheres initialized with zero velocity and random positions within a $10\text{-}\mu\text{m}$ ball subject to a minimum-separation constraint to prevent collisions. Figure 7 shows a snapshot of the velocity potential isosurfaces calculated in one such simulation. Even with mutual interactions, the shape of each isosurface remains consistent with the presence of a dipolar field oriented along the microspheres' velocity. Again, due to the localization assumption used to justify Eq. (6), each system predominantly translates a finite distance in accordance with the results found for a single microsphere in Fig. 3. To quantify small changes in the geometry of a system, we compute V_h , the volume of the convex hull containing each microsphere, at every time step in the simulation [23]. Figure 8 shows the fractional change in the hull volume,

$$\Delta V_h = \frac{V_h(t) - V_h(0)}{V_h(0)}, \quad (33)$$

for 20 such systems after smoothing with a weighted moving average. Curves ending above and below zero indicate larger and smaller hull volumes (system expansion and contraction). We note from Fig. 8 a greater tendency for random clouds to expand; the effective dipole-dipole interaction between particles with $\mathbf{d}_{ij} \perp \mathbf{k}$ gives purely repulsive forces, while the interaction between particles with $\mathbf{d}_{ij} \parallel \mathbf{k}$ gives both repulsive

and attractive effects depending on σ and the relative phase of the oscillating microsphere velocities.

VI. CONCLUSIONS

This work lends a novel, fine-grained approach to the study of acoustic response via integral equation methods. By considering a potential representation in terms of spherical harmonics on the surfaces of microspheres coupled to a standard molecular dynamics scheme, we obtain a description of the microspheres' dynamics under the effect of ultrasound pulses without resorting to time-average approximations, though the confined microsphere geometries under consideration allow us to neglect small effects arising from time delays in scattering. We have shown that the net effect of an ultrasound pulse on a single microsphere consists of a translation that we can tune through careful control of pulse parameters. Additionally, systems with multiple incident waveforms tend to confine microspheres to nodes in the pressure field governed by acoustic interference. Finally, in the dynamics of systems with many microspheres, we have observed the effect of

weak interparticle transient effects induced by the driving acoustic pulse. These effects can produce both expansion and contraction of a cloud of microspheres, in addition to the overall translation.

Prior work in this area [24,25] makes use of deformable bubble boundaries about fixed locations. Incorporation of these methodologies to our theoretical model naturally offers possibilities for future research, as does the addition of retardation effects. Additionally, we expect a straightforward approach to experimental confirmation of the results presented here. Optical tracking of tracer particles [26] has demonstrated its effectiveness in similar fluid-trajectory studies and would readily adapt to track physical analogues of our theoretical microspheres.

ACKNOWLEDGMENTS

The authors gratefully acknowledge NSF Grants No. 1250261 and No. 1408115 for financially supporting this project as well as iCER and the High Performance Computing facility at Michigan State University for their computational resources.

-
- [1] P. C. Waterman, *J. Acoust. Soc. Am.* **45**, 1417 (1969).
 - [2] Y. Ding, A. Forestier, and T. H. Duong, *J. Acoust. Soc. Am.* **86**, 1566 (1989).
 - [3] Z. Ye, *J. Acoust. Soc. Am.* **101**, 1945 (1997).
 - [4] M. J. Blomley, J. C. Cooke, E. C. Unger, M. J. Monaghan, and D. O. Cosgrove, *Br. Med. J.* **322**, 1222 (2001).
 - [5] J. S. Allen, D. J. May, and K. W. Ferrara, *Ultrasound Med. Biol.* **28**, 805 (2002).
 - [6] S. Hernot and A. L. Klibanov, *Adv. Drug Delivery Rev.* **60**, 1153 (2008).
 - [7] X. Ding, J. Shi, S.-C. S. Lin, S. Yazdi, B. Kiraly, and T. J. Huang, *Lab Chip* **12**, 2491 (2012).
 - [8] L. Ye, J. Liu, P. Sheng, and D. A. Weitz, *Phys. Rev. E* **48**, 2805 (1993).
 - [9] L. V. King, *Proc. R. Soc. London A* **147**, 212 (1934).
 - [10] F. Borgnis, *Rev. Mod. Phys.* **25**, 653 (1953).
 - [11] N. A. Gumerov and R. Duraiswami, *J. Acoust. Soc. Am.* **112**, 2688 (2002).
 - [12] A. A. Doinikov, *J. Acoust. Soc. Am.* **116**, 821 (2004).
 - [13] A. A. Doinikov, R. Manasseh, and A. Ooi, *J. Acoust. Soc. Am.* **117**, 47 (2005).
 - [14] Y. A. Ilinskii, M. F. Hamilton, and E. A. Zabolotskaya, *J. Acoust. Soc. Am.* **121**, 786 (2007).
 - [15] S. Azizoglu, S. Koc, and O. Buyukdura, *SIAM J. Appl. Math.* **70**, 694 (2009).
 - [16] L. Tsang, K. H. Ding, S. E. Shih, and J. A. Kong, *J. Opt. Soc. Am. A* **15**, 2660 (1998).
 - [17] J. Li, D. Dault, and B. Shanker, *J. Acoust. Soc. Am.* **135**, 1676 (2014).
 - [18] M. K. Myers and J. S. Hausmann, *J. Acoust. Soc. Am.* **91**, 2594 (1992).
 - [19] L. Landau and E. Lifshitz, *Fluid Mechanics*, Vol. 6 (Elsevier Science, Amsterdam, 2013), pp. 14–31.
 - [20] M. J. Caola, *J. Phys. A: Math. Gen.* **11**, L23 (1978).
 - [21] L. F. Greengard, The rapid evaluation of potential fields in particle systems, Ph.D. thesis, Yale University, New Haven, CT, 1987.
 - [22] H. Childs, E. Brugger, B. Whitlock, J. Meredith, S. Ahern, D. Pugmire, K. Biagas, M. Miller, C. Harrison, G. H. Weber, H. Krishnan, T. Fogal, A. Sanderson, C. Garth, E. W. Bethel, D. Camp, O. Rübél, M. Durant, J. M. Favre, and P. Navrátil, in *High Performance Visualization—Enabling Extreme-Scale Scientific Insight* (Chapman and Hall/CRC, Boca Raton, FL, 2012), pp. 357–372.
 - [23] E. Jones, T. Oliphant, P. Peterson, *et al.*, “SciPy: Open source scientific tools for Python”, (2001–) [online, accessed 10-14-2014].
 - [24] Z. Zeravcic, D. Loshe, and W. Van Saarloos, *J. Fluid Mech.* **680**, 114 (2011).
 - [25] A. Tiwari, C. Pantano, and J. B. Freund, *J. Fluid Mech.* **775**, 1 (2015).
 - [26] F. Toschi and E. Bodenschatz, *Annu. Rev. Fluid Mech.* **41**, 375 (2009).